JOURNAL OF Applied Polymer SCIENCE

Correlation of the morphology and thermooxidative degradation behavior of poly(ethylene terephthalate)-nitrile butadiene rubber-polycarbonate ternary blends

Hamidreza Ali-Asgari Dehaghi, Amin Boudaghi Malidareh, Milad Edraki, Navid Sedaghat, Ardalan Farokhzad

Department of Polymer Engineering, South Tehran Branch, Islamic Azad University, 1777613651, Tehran, Iran

Correspondence to: N. Sedagaht (E-mail: navid2717@yahoo.com)

ABSTRACT: In this study, we prepared ternary poly(ethylene terephthalate) (PET)–nitrile butadiene rubber (NBR)–polycarbonate (PC) blends through a molten mixing procedure, and with a corotating extruder, we studied the morphology and thermodynamic properties of each purified polymer and the binary and ternary blends with different compositions. Dynamic mechanical analysis of both the PET–PC and PET–NBR samples showed individual loss peaks for each component, but in different ternary samples, the effects of different percentages of components (PC–PC and PET–NBR) were observed; this revealed changes in the loss peak locations. Individual loss peaks of PET and PC in the ternary PET–NBR–PC blends (81/9/10 and 63/30/7)—proof of the miscibility of the samples—were also observed in this study. The thermal properties of the samples were measured and examined with the thermogravimetric analysis and differential thermogravimetry testing methods. The activation energy and order of reaction values for the samples under an air atmosphere with single-rate methods of heating were studied. Finally, the relation between the type of morphology and the thermal degradation behavior was investigated. © 2018 Wiley Periodicals, Inc. J. Appl. Polym. Sci. **2018**, *136*, 47171.

KEYWORDS: degradation; morphology; thermal properties

Received 3 April 2018; accepted 27 July 2018

DOI: 10.1002/app.47171

INTRODUCTION

Polymeric blending is one of the simplest and most economical methods of producing polymers products. At this point, polymer technology scientists have considered blending from both scientific and industrial viewpoints.[1] Within the last few years, new elements have been introduced to form and control the morphologies of these blends[2,3] although correlations between such elements and the thermal and mechanical properties of the products has not yet been obtained. Plastic toughening without a decrease in the mentioned properties, such as the modulus, tensile strength, and thermal stability, has been an objective for polymer scientists. For this purpose, it is essential to determine the dependencies of the polymer morphologies and properties. Poly(ethylene terephthalate) (PET), as an engineering plastic, has seen a rapid growth in recent years. However, it is still necessary to enhance its toughness in many of its applications.[4] One of the methods for reaching this value is the modification of its properties via its blending with an elastomer.[5] The addition of an elastomer leads to marked decreases in the modulus and thermal stability of the blend for the sake of special properties. Indeed, it is significant to add a third component to eradicate these defects. The correlation of the morphology with the thermal and thermooxidation degradation behavior of polymer blends has not been efficiently studied.[6,7] Moreover, it is crucial to determine the correlation between bottlenecks and key questions of the blending process. Polymer blending could lead to improvements and reductions in the thermal stability.[8] Polymer blends include important characterization factors of thermal degradation, such as miscibility, compatibilzation effects, proportion effects of the component, and also the formation of crosslinking structures and copolymers.[9] Lizymol *et al.*[10] investigated the miscibility effect on polymer blends in thermal degradation behavior. The outcomes for poly(vinyl chloride)–ethylene–vinyl acetate, ethylene–vinyl acetate–styrene acrylonitrile, and poly(vinyl chloride)–acetate–styrene acrylonitrile blends were improvements in the thermal stability properties for miscible blend of poly(vinyl chloride)–ethylene–vinyl acetate, but it has been reported that the two other samples were not considerable. Roeder *et al.*[9] scrutinized the effects of a polypropylene-grafted maleic anhydride compatibilizer on the morphology and thermal behavior of polypropylene–polyethylene and polypropylene–polyurethane blends and reportedly came up with a major response to the formation of the phase morphology and reported that the thermal stability of these blends was a functionality of the morphology. Jose and Tomas

considered polyamide 12–styrene–ethylene–butadiene–styrene and polyamide 12–styrene–ethylene–butadiene–styrene grafted maleic anhydride blends and reported that the relation between their thermal stability and morphology was very intense. The result demonstrates that the use of compatibilizer resulted in a cocontinuous morphology and more qualified thermal properties. Natasa *et al.*[12] pondered the thermooxidation degradation kinetics of poly(vinyl chloride)–chlorinated polyethylene blends with the Kissinger, Kissinger–Akahira–Sunose (KAS), and Friedman models; they also determined the kinetic parameters. Additionally, the component composition effects were contemplated and determined.

In this study, we aimed to figure out the thermal degradation kinetics and the correlation between the morphology and thermal behavior of binary PET–nitrile butadiene rubber (NBR) and PET–polycarbonate (PC) and ternary PET–NBR–PC and study the influence of the weight percentage ratio of the NBR and PC phase. Also, to survey the thermal properties of both the PET–NBR and PET–PC blends, we found it necessary to add three components together. In previous studies, the correlation between such elements and the thermal properties and morphology were not investigated.

To determine and compare the kinetic parameters in this study, we used the Friedman, Freeman-Carroll, and Chang nonisothermal differential methods and KAS integral methods. Eventually, we found distinguishing features among all of the samples.

EXPERIMENTAL

Materials

PET granules were obtained from Texpet Co. (Korea). The polymers used in this study were formed of acrylonitrile–butadiene rubber containing 33 wt % acrylonitrile from Korea Kumho Petrochemical Co. (Korea). PC, with the trade name Makrolon 2858, was purchased from Bayer Co. (Germany).

Sample Preparation

Blends of different systems and compositions were concurrently prepared with a Brabender corotating twin-screw extruder (diameter of screw = 2 cm, length/diameter ratio = 40). Before processing, PC was dried in a vacuum oven for about 18 h at 80°C, whereas PET remained there for 24 h at 120°C. The barrel of the extruder had six temperature-control zones from 235°C (hopper) to 260°C (die), and the screw velocity was set at 60 rpm. Consequently, the extrudates were quenched in a cooling water bath and pelletized through a granulator. To investigate the role of the blend composition, six binary and ternary blends were prepared, as illustrated in Table I.

Characterization Method

Scanning electron microscopy (SEM) was performed with a Cambridge apparatus equipped with a 17 kV energy beam. The prepared samples were cryogenically fractured in liquid nitrogen and coated via a gold vapor deposition method with a vacuum sputterer before SEM observation.

The degradation of the blends was analyzed with an STA PT1600 thermogravimetry (TG) analyzer under an air atmosphere.

Table I. Component Percentages of Each Sample

		Composition (%)		
Code	Sample	PET	NBR	PC
PC10	PET–PC	90	0	10
PC20	PET–PC	80	0	20
PC30	PET–PC	70	0	30
NB10	PET–NBR	90	10	0
NB20	PET–NBR	80	20	0
NB30	PET–NBR	70	30	0
P1	PET–NBR–PC	81	10	9
P2	PET–NBR–PC	72	20	8
P3	PET–NBR–PC	63	30	7
P4	PET–NBR–PC	81	9	10
P5	PET–NBR–PC	72	8	20
P6	PET–NBR–PC	63	7	30

Nonisothermal analysis was performed in the temperature range 25–850°C at different heating rates (10, 20, and 30°C/min). The air flow was maintained at 33 mL/min, and samples of about 20 mg were used for all measurements.

A TA Instruments Tritec DMA2000 dynamic mechanical analyzer was used to evaluate the dynamic mechanical properties of the pure PET and PC30, NB30, P1, P3, P4, and P6 blends. The specimens were 10 mm wide by 20 mm long by 3 mm thick. They were subjected to three-point bending at a vibration frequency of 1 Hz and a heating rate of 5°C/min under a nitrogen atmosphere.

Kinetic Methods

The recorded original degradation traces were further allowed to be processed according to the following mathematical expression to characterize the thermal degradation kinetics of these blend samples:[13]

$$d\alpha/dT = A\exp(-E/RT)(1-\alpha)^n \quad (1)$$

where α is the weight loss of the copolyester film sample having undergone thermal degradation at an experimental time *t*, $d\alpha/dt$ is the thermal degradation rate or weight loss rate, *A* is a frequency factor, *n* is the order of the thermal degradation reaction, E_a is the thermal degradation reaction activation energy, *R* is the gas constant (8.3136 J mol^{-1} K^{-1}), and *T* is the absolute temperature (K).[14] Furthermore, three characterization methods proposed by Friedman,[15] Freeman-Carroll,[16] and Chang,[17] respectively, were applied to explore the thermal degradation kinetic parameters and mechanisms:

$$\mathrm{Ln}(d\alpha/dt) = \ln A + n\ln(1-\alpha) - E/(RT) \quad (2)$$

Chang method used the following form of eq. (2):

$$\ln[(d\alpha/dt)/(1-\alpha)^n] = \ln A - E/(RT) \quad (3)$$

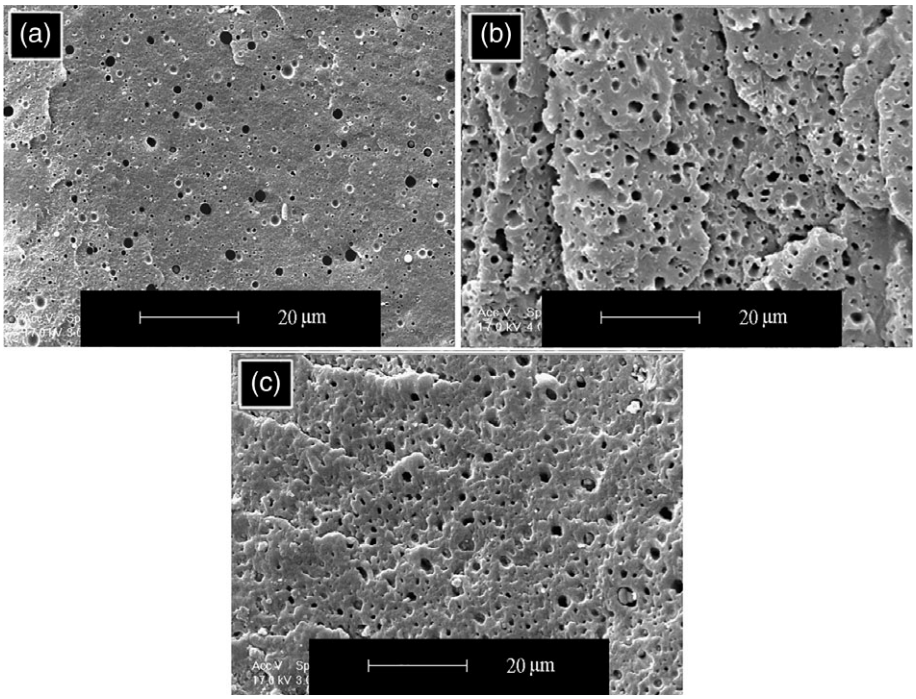

Figure 1. SEM micrographs of the effects of PC and NBR on the morphology of the samples with different PC contents: (a) PC10, (b) PC20, and (c) PC30.

Furthermore, a mathematical plot of $\ln[(d\alpha/dt)/(1-\alpha)^n]$ against $1/T$ can yield a straight line if n is selected correctly. The slope and intercept of the plot can provide the E_a/R and ln A values, respectively.

The Freeman-Carroll method applies another deduced equation as follows:

$$\Delta\ln(d\alpha/dt)/\Delta\ln(1-\alpha) = n-(E/R)\Delta(1/T)/\Delta(1-\alpha) \quad (4)$$

When plotting $\Delta\ln(d\alpha/dt)/\Delta\ln(1-\alpha)$ against $\Delta(1/T)/\Delta\ln(1-\alpha)$, one can obtain a straight line with a slope and intercept equal to E_a/R and n, respectively. The values of $\Delta\ln(d\alpha/dt)$ and $\Delta\ln(1-\alpha)$ can be taken at regular intervals of $1/T$, where $\Delta(1/T)$ is accordingly fixed as 2×10^{-6} K^{-1}.

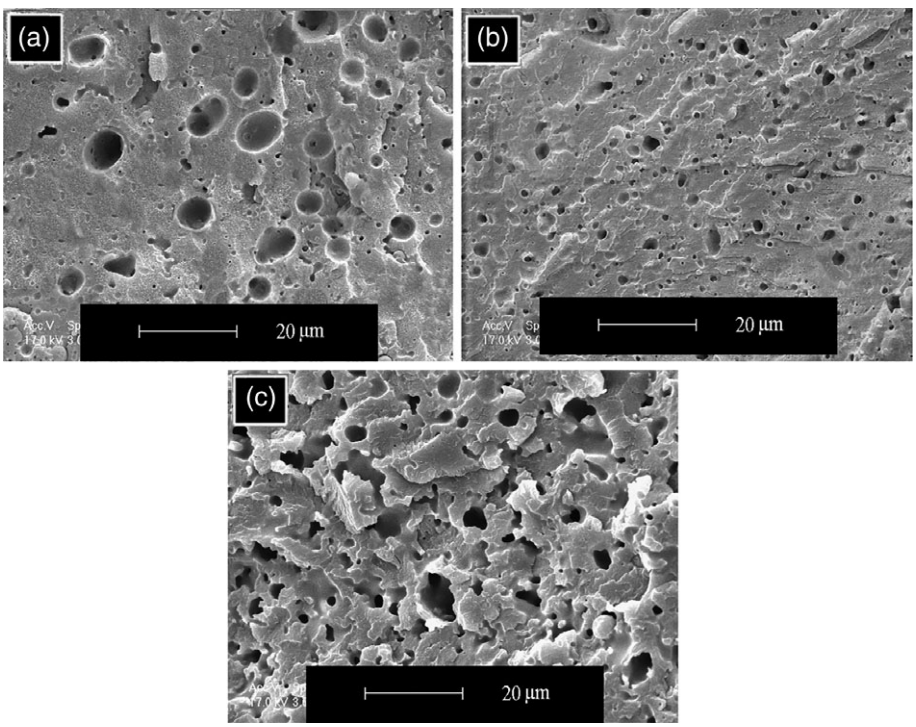

Figure 2. SEM micrographs of the effects of PC and NBR of the samples with different PC contents: (a) NB10, (b) NB20, and (c) NB30.

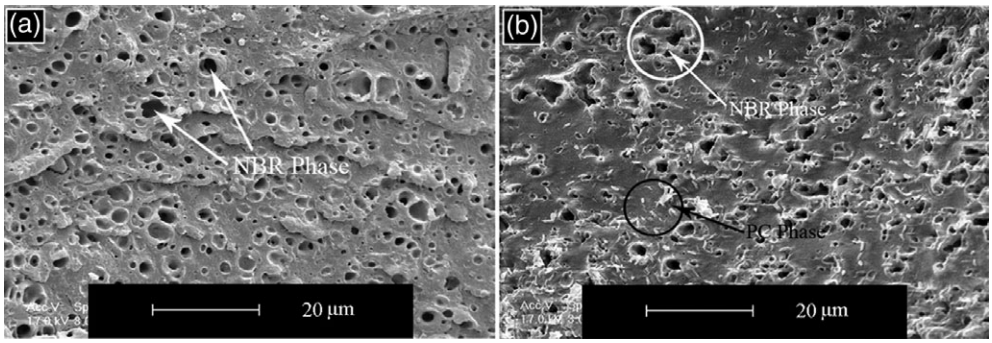

Figure 3. SEM micrographs of the effects of PC and NBR of the samples with different PC contents: (a) PC10 and (b) PC30 with 10% NBR.

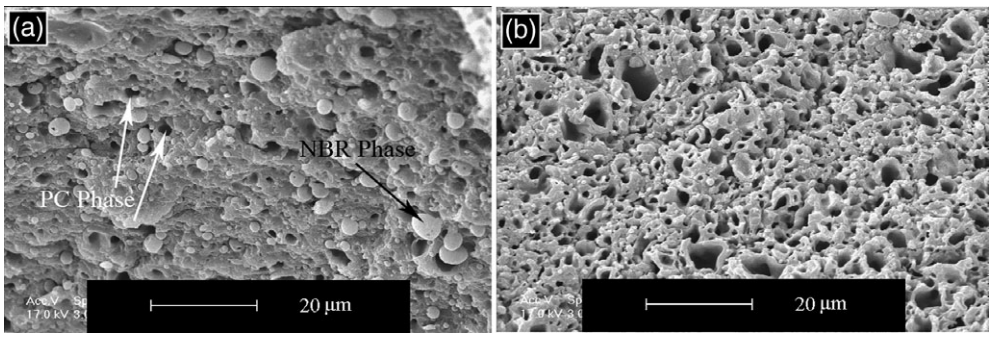

Figure 4. SEM micrograph of the effects of PC, PET, and NBR on the morphology of the samples: (a) P4 and (b) P6.

Isoconversional Methods

These methods are known to allow for model-independent estimates of E_a. Their use allows the investigation of the dependence of E_a on the conversion degree.

Flynn–Wall–Ozawa (FWO) Method. The isoconversional integral method, suggested independently by Flynn and Wall[18] and Ozawa, uses Doyle's[19] approximation of the temperature integral. This method is based on the following equation:

$$\mathrm{Ln}\beta = \ln[AE/R{\cdot}g(\alpha)] - 5.331 - 1.053(E/RT) \quad (5)$$

where

$$g(\alpha) = \int_0^{\alpha} \frac{d\alpha}{f(\alpha)}$$

is the integral conversion function f(α) is the differential conversion function and b = dT/dt = const. Thus, for a constant α, the plot of ln β versus $1/T$ obtained from thermograms recorded at several heating rates should be a straight line whose slope allows for the evaluation of E_a.

KAS Method.[20,21] This isoconversional integral method is based on the Coats–Redfern[22] approximation of the temperature integral. It was exposed that

$$\ln(\beta/T^2) = \ln[AR/Eg(\alpha)] - E/(RT) \quad (6)$$

Thus, for at a constant α, the plot of $\ln(\beta/T^2)$ versus $1/T$, obtained from thermograms recorded at several heating rates, should be a straight line whose slope can be used to evaluate E_a.

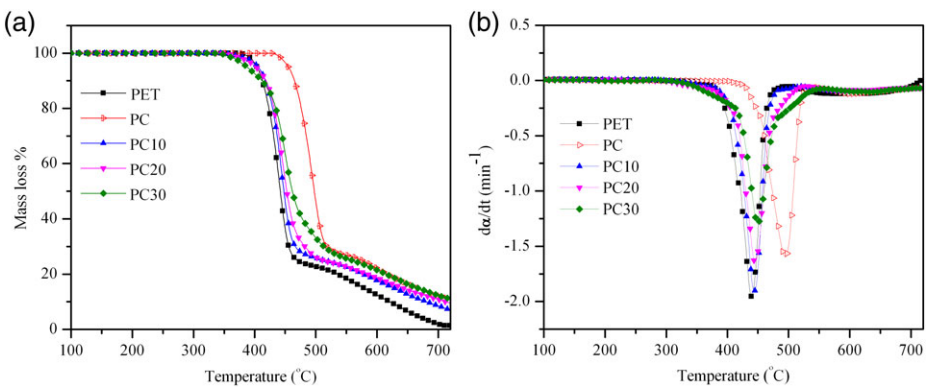

Figure 5. (a) Mass percentage (TG) and (b) DTG curves versus the temperature for the PET, PC, PC10, PC20, and PC30 samples. [Color figure can be viewed at wileyonlinelibrary.com]

Table II. T_{onset}, T_{max}, and Char Values of the Samples

Sample	T_{onset}	T_{max}	Char at 800°C (%)
PET	403.71	439.21	1.36
PC	455.03	494.05	6.02
NBR	347.93	450	0.04
PC10	405.11	444	1.5
PC20	402.10	445.39	4.91
PC30	387.20	450	6
NB10	370.60	431.93	0.27
NB20	395.32	428.03	4.63
NB30	385.41	423.35	6.81
P1	394.13	428.95	3.32
P3	359.65	435.30	5.27
P4	388.79	427.10	1.52
P6	380.22	424.53	5.56

RESULT AND DISCUSSION

Morphological Study

Figures 1 and 2 illustrate the SEM binary blend images of the composition effects of PC and NBR on the morphology. In Figure 1(A–C), the composition effect of PC is shown. The PC phase in blends was extracted by diethylenetriamine solvent, and a matrix-dispersed morphology was depicted. When the composition ratio of PC20 added to the sample was increased, the cavity witnessed an increase, and with addition of PC to 30 wt %, the dispersed phase shrunk. The irregular interphase revealed strong interactions between PET and PC. In Figure 2(A–C), the composition ratio of NBR is illustrated in these blends. NBR was etched by acetone. Although a lower content of NBR was visible in the NB10 sample, it was astonishing that the particle size was far bigger than those of the NB20 and NB30 samples. For NB20, the particle size of the dispersed phase was smaller, and it had a better dispersion. The morphology of NB30 was close to a phase-inversion status. Figure 3(A,B) indicates the morphologies of the P1 and P3 samples, respectively. The NBR phase was viewed as dark holes. Because of the presence of 10 wt % NBR, the occurrence of transesterification and an exchange reaction during the mixing process led to the production of a random copolymer, and the morphology of P1 was much more miscible than that of P3 with 30 wt % PC. As a result, the PC seemed to be soluble in the PET matrix.[23,24] Transesterification was acknowledged to have experienced a reduction because of the addition of 10–30 wt % PC. Also, PC could be illustrated as a rod particle in the PET matrix. Conversely, the amount of these rods was still under the PC content used in the blend; this might have been a result of the solubility between PET and PC mentioned before. Figure 4 (A,B) features the morphologies of the P4 and P6 samples. The NBR phase in P4 was observed spheroid particles, and the sample morphology was observed as two dispersed phases. The NBR spheres were almost the same size and did not show a good dispersion, however. PC addition ratios to 30 wt % in the P6 sample altered and changed the morphology into a cocontinuous one.

Thermooxidation Degradation

TG analysis was used to examine the thermooxidation behavior in this study. Figure 5(A,B) presents the TG and differential thermogravimetry (DTG) curves of the pure samples of PET and PC along with the effects of the composition ratio of PC in the PC10, PC20, and PC30 blends. Information such as the initial degradation temperature was obtained from the TG figures; moreover, the same applied to the degradation procedure. Furthermore, data for the degradation stage, such as the temperature at the maximum degradation rate (T_{max}), were achieved by the numerical derivation of the TG data and curve drawing of the DTG characterization. All of the sample data were reported accordingly (Table II). The DTG curve for the pure PET specified two peaks for the occurrence of a two-stage degradation.[25] According to the data for PET from the TG test, the first stage of degradation started at 516°C with a 71% mass loss. On the other hand, PC was most likely to from a branch product and, consequently, to produce an intermediate char-form composition. The layers of the char acted as an oxygen barrier for the following thermal degradation process and resulted in a reduction in the degradation rate of PC.[26] The transesterification and exchange reactions during the melt-blending process at high temperatures created a random copolymer, and there was a compatibilization reaction in the blends.[24] The initial degradation temperature decreased at a conversion (α) under a value of 0.05 as the PC amount increased from 10 to 30 wt % (PC10, PC20, and PC30) in the blends. The reason for this

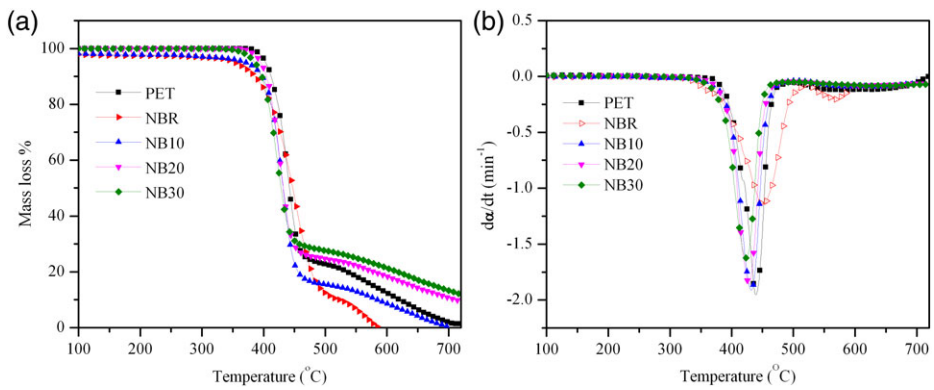

Figure 6. (a) Mass percentage (TG) and (b) DTG curves versus the temperature for the PET, NBR, NB10, NB20, and NB30 samples. [Color figure can be viewed at wileyonlinelibrary.com]

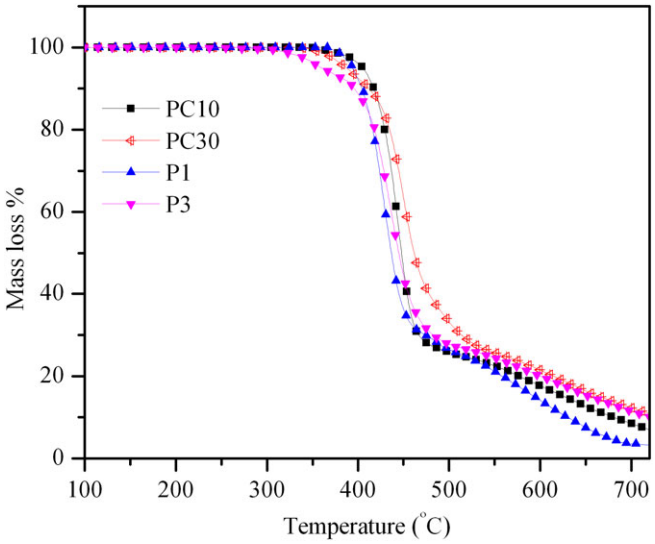

Figure 7. Mass percentage (TG) curves versus the temperature for the PC10, PC20, P1, and P3 samples. [Color figure can be viewed at wileyonlinelibrary.com]

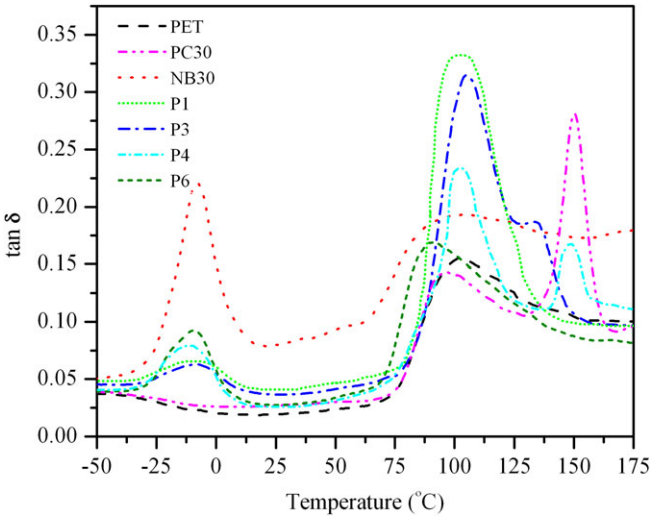

Figure 9. Loss factor (tan δ) values for the pure PET sample, binary PC30 and NB30 samples, and ternary P1, P3, P4, and P6 samples. [Color figure can be viewed at wileyonlinelibrary.com]

phenomenon was an increase in the rate of the transesterification reaction occurring at a temperature around 300°C.[27] However, the thermal stability increased because of PC addition at a higher conversion ($\alpha \geq 0.05$).[28] As mentioned, the tendency to produce a branch product in PC led to char production.[26] The effects of the proportional miscibilities of the PC10, PC20, and PC30 blends in the results of the DTG were spectacular. This order of the DTG curves in these blends displayed an overlap between the amounts of PC and PET. T_{max} escalated (Table II) with increasing weight percentage of PC. Figure 6(A,B) shows the TG and DTG curves of the composition ratio effect of NBR in the NB10, NB20, and NB30 blends. Rubbers generally have a low thermal stability; thus, the addition of rubber to the polymers with a high thermal stability was most likely to result in a reduction in the thermal properties. The results obtained from the TG curve show that with an increase in the NBR composition ratio from 10 to 30 wt %, the initial degradation temperature and the thermal stability were indicative of a reduction thereafter. In addition, we observed in the DTG curves that T_{max} decreased with an addition to the composition ratio of NBR for these blends. A rise led to an increase in the char formation in the end of blend degradation. Notably, the formed char gave rise to a reduction in the mass loss ratio at high conversion because of the oxygen-barrier properties. Holistically, the conclusion drawn denoted that at a low amount of NBR, the degradation mechanism was to a greater extent influenced by the PET matrix. In the TG curves in Figure 7, the

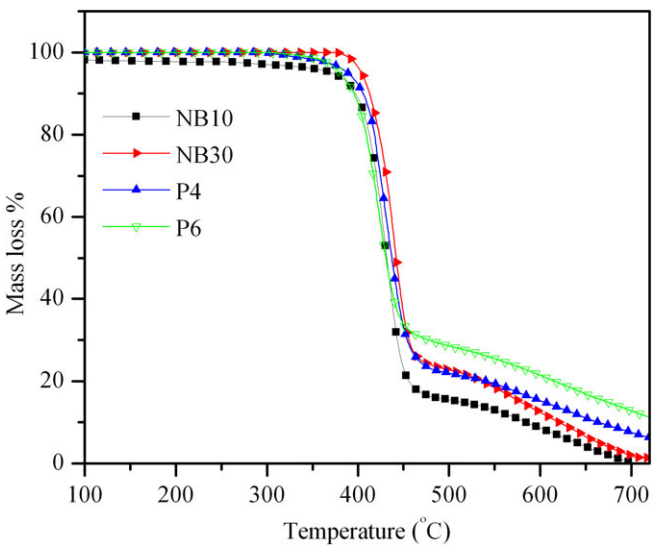

Figure 8. Mass percentage (TG) curves versus the temperature for the NB10, NB30, P4, and P6 samples. [Color figure can be viewed at wileyonlinelibrary.com]

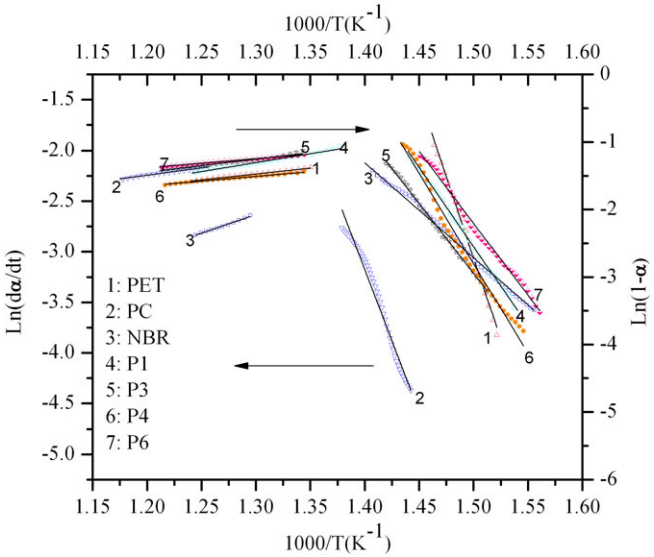

Figure 10. Two sets of curves: the Friedman method plots of $\ln(d\alpha/dt)$ versus $1/T$ and $\ln(1-\alpha)$ versus $1/T$. [Color figure can be viewed at wileyonlinelibrary.com]

Table III. E_a Values Determined with the Friedman, Freeman-Carroll, and Chang Methods

	Friedman method				Freeman-Carroll method				Chang method			
Sample	E_a	n	Ln A	r	E_a	n	Ln A	r	E_a	n	Ln A	r
PET	229.8	0.68	38.4	0.9953	250.1	0.60	40.3	0.9989	225.9	0.81	37.8	0.9992
PC	277.5	0.61	43.3	0.9959	299.4	0.53	46.1	0.9888	272.4	0.77	42.4	0.9994
NBR	113.5	1.19	17.8	0.9908	136.7	1.12	20.4	0.9865	197.4	0.99	16.4	0.9989
PC10	220.3	0.64	36.3	0.9938	242.7	0.67	38.9	0.9856	216.4	0.75	35.1	0.9991
PC20	196.6	0.61	31.9	0.9977	223.9	0.52	33.6	0.9945	193.9	0.72	30.4	0.9999
PC30	222.8	0.40	36.1	0.9974	245.9	0.33	37.9	0.9812	218.7	0.44	35.6	0.9988
NB10	194.6	0.89	32.5	0.9978	216.3	0.80	34.6	0.9846	191.2	0.93	31.3	0.9991
NB20	248.1	0.56	41.3	0.9969	265.6	0.50	44.1	0.9991	245.7	0.88	39.9	0.9999
NB30	207.3	0.57	35.2	0.9943	225.4	0.52	38.5	0.9872	205.5	0.89	34.2	0.9976
P1	188.9	0.62	31.5	0.9993	209.3	0.54	34.7	0.9819	185.8	0.69	30.1	0.9996
P3	182.1	0.51	29.8	0.9905	203.6	0.43	32.6	0.9819	179.2	0.55	27.9	0.9969
P4	188.6	0.67	30.9	0.9948	207.8	0.60	33.9	0.9956	186.1	0.71	28.8	0.9991
P6	177.6	0.57	27.8	0.9939	198.1	0.49	30.8	0.9989	173.7	0.60	26.6	0.9969

binary PC10 and PC30 samples are indicated and compared with the ternary P1 and P3 samples. We observed that the mass loss was initiated from a lower ratio in a P3 sample including the 30 wt % PC phase, such as PC30. As the ratio was enhanced because of the higher thermal stability of PC, a higher resistance was observed in the P3 sample. Additionally, char formation was observed for the high conversion. The TG curves for the binary NB10 and NB20 samples are compared with ternary P4 and P6 samples in Figure 8. The thermal stabilities for the ternary P4 and P6 samples were greater than those of the binary samples according to the presence of PC. The degradation mechanism was a function of the degradation of the NBR phase, similar to binary NB30, because of the greater amount of NBR phase in the P6 blend. Table II presents the residual measurements for all of the samples.

Dynamic Mechanical Properties

Figure 9 indicates the loss factors of the pure PET, binary PC30 and PC30, and ternary P1, P3, P4, and P6 samples. The temperature of one peak was observed for the pure sample PET as the glass-transition temperature (T_g). A peak related to each component was individually viewed for PC30 and NB30. The board peak was observed in the NB30 sample for the sake of a low difference in the component solubility parameter and the presence of the acrylonitrile polar function in NBR, the tendency of which to react to the end group of PET led to a low compatibility. Similarly, the transesterification led to a proportional compatibility in the PC30 sample during the mixing process and the production of random copolymer. As a result, the component loss peaks were close to those of the blends.[24] Although the change in the T_g value and the closeness of the T_g components indicated a proportional miscibility of these samples, the results of the

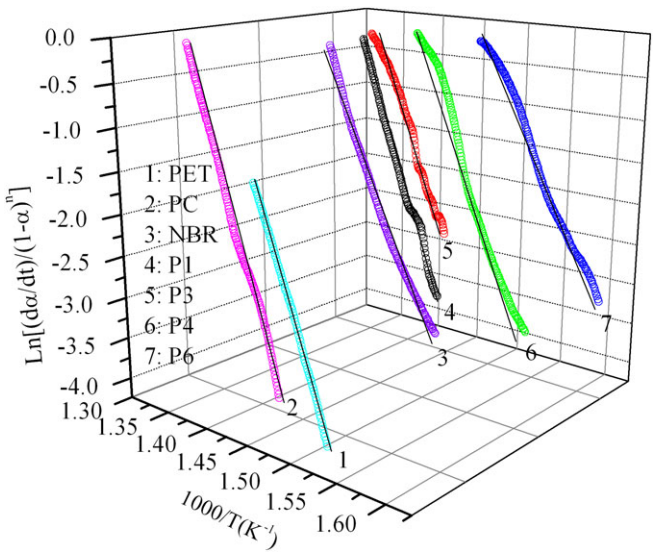

Figure 11. Chang plot for the PET, PC, NBR, P1, P3, P4, and P6 samples: $\{\ln[(d\alpha/dt)/(1-\alpha)^n]$ and $103(T^{-1})\}$. [Color figure can be viewed at wileyonlinelibrary.com]

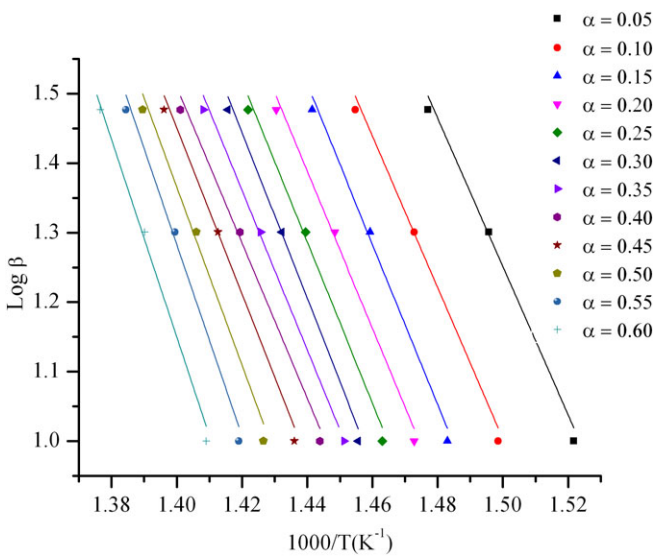

Figure 12. Kissinger plots for sample P1 (log β spot vs $1/T$). [Color figure can be viewed at wileyonlinelibrary.com]

Table IV. E_a Values Determined with the KAS and FWO Methods for the PET and P1, P3, P4, and P6 Samples

	PET				P1			
	KAS		FWO		KAS		FWO	
Conversion α	E_a	r	E_a	r	E_a	r	E_a	r
0.05	184.28	0.9996	181.43	0.9898	175.47	0.9995	172.60	0.9880
0.10	205.53	0.9997	202.80	0.9888	197.66	0.9998	194.90	0.9883
0.15	211.74	0.9989	207.44	0.9985	210.35	0.9986	207.44	0.9888
0.20	215.80	0.9998	218.59	0.9857	223.02	0.9989	220.21	0.9857
0.25	209.35	0.9984	212.09	0.9992	228.55	0.9975	225.79	0.9846
0.30	220.81	0.9997	220.91	0.9987	234.13	0.9968	231.36	0.9845
0.35	224.39	0.9987	221.61	0.9888	237.68	0.9969	234.84	0.9888
0.40	232.27	0.9986	229.50	0.9976	248.86	0.9956	245.99	0.9868
0.45	232.75	0.9943	229.97	0.9952	253.86	0.9988	251.10	0.9898
0.50	236.33	0.9935	233.45	0.9896	263.08	0.9991	260.39	0.9890
0.55	242.78	0.9946	239.95	0.9963	272.69	0.9982	269.91	0.9878
0.60	251.37	0.9989	248.55	0.9888	299.21	0.9923	296.39	0.9899

P3				P4				P6			
KAS		FWO		KAS		FWO		KAS		FWO	
E_a	r	E_a	r	E_a	r	E_a	r	E_a	r	E_a	R
170.98	0.9989	168.19	0.9846	193.55	0.9987	190.72	0.9809	198.96	0.9943	196.06	0.9819
163.30	0.9975	160.53	0.9845	228.08	0.9986	225.32	0.9808	231.72	0.9935	229.04	0.9818
199.94	0.9968	197.22	0.9888	265.45	0.9913	262.71	0.9985	326.39	0.9946	323.56	0.9965
216.57	0.9986	213.71	0.9868	280.22	0.9925	277.34	0.9857	352.84	0.9989	350.04	0.9857
235.74	0.9943	232.99	0.9888	274.96	0.9936	272.24	0.9932	361.55	0.9956	358.86	0.9952
247.87	0.9935	245.06	0.9985	277.97	0.9968	275.25	0.9857	363.32	0.9988	360.49	0.9857
260.24	0.9988	257.37	0.9857	276.86	0.9969	274.09	0.9826	355.93	0.9991	353.06	0.9886
275.48	0.9991	272.70	0.9992	272.73	0.9956	269.91	0.9845	349.18	0.9982	346.32	0.9875
286.17	0.9982	283.38	0.9987	276.51	0.9988	273.63	0.9888	342.91	0.9923	340.05	0.9878
304.66	0.9923	301.96	0.9880	273.32	0.9911	270.61	0.9868	355.56	0.9981	352.82	0.9848
352.09	0.9918	349.34	0.9883	271.32	0.9901	268.52	0.9923	376.90	0.9962	374.19	0.9933
502.30	0.9981	499.60	0.9888	277.26	0.9921	274.56	0.9918	466.75	0.9903	464.07	0.9908

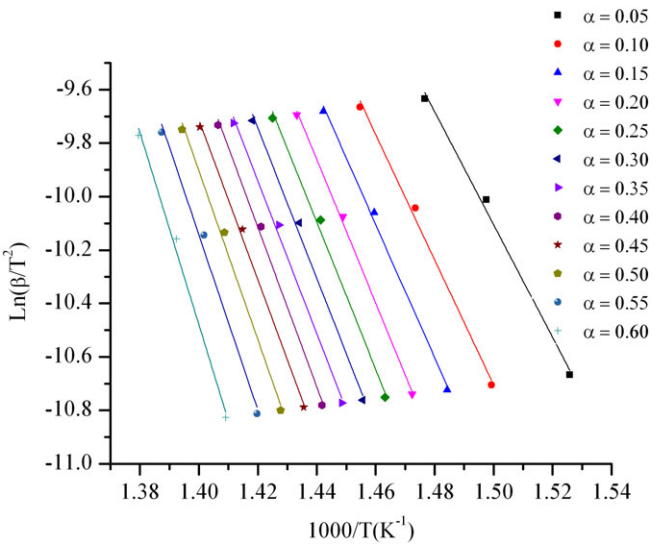

Figure 13. FWO plots for sample P1 (log β spot vs 1/*T*). [Color figure can be viewed at wileyonlinelibrary.com]

dynamical mechanical tests for the ternary sample of P1 including NBR, PC, and PET presented two peaks: the first was at temperatures below zero and belonged to the loss component of NBR, whereas the other one was higher than the other curves belonging to the loss of PET and PC on the basis of the proper solubility and the production of a random copolymer during the melt-mixing process. Surreesm reported the properties of a P3 sample for PET and PC components and found an overlapping peak; this indicated a lower and proportional solubility comparing to the P1 sample, whereas for the P6 sample, the dynamic mechanical test results for PET and PC displayed more broad peak with a lower height compared to P1 and P3 because of a lower modulus of the NBR phase; this facilitated the movement of branches. The T_gs for the samples are reported in Table II.

Investigation of Nonisothermal Degradation

Because the main purpose of this research was to scrutinize the thermooxidation degradation kinetics and obtain the kinetic parameters E_a, n, and A (ln A), the decomposition process of the differential models of Friedman, Chang, and Freeman-Carroll was used.[15–17] In addition, the models of KAS and FWO were practiced to measure the values of E_a from the two models of integration.[18–21] The measurements of the kinetic parameters obtained from these models clearly determined the component ratio effect on the thermooxidation degradation behavior. Higher correlation coefficients (rs) indicated that the model was in good agreement with the experimental data. The kinetic parameters of E_a and n, respectively, showed the thermal stability and reaction rate during the decomposition process. Figure 10 includes the results of the degradation modeling of the blends at four compositions by the Friedman technique, along with the experimental data. Two sets of curves are presented in the figure; one of them is the plot of $\ln(d\alpha/dt)$ against $1/T$, which gives the E_a values, and the other set is the plot of $\ln(1-\alpha)$ against $10^3(T^{-1})$, which gives the n values. The characteristic degradation parameters and rs are reported in Table III. The values of E_a and n obtained from the Friedman plot were lower than those obtained with the Chang and Freeman-Carroll methods. Figure 11 illustrates the results of the modeling of the experimental data with the Chang technique. As the axes representing $\ln[(d\alpha/dt)/(1-\alpha)^n]$ and $10^3(T^{-1})$ were the same for all of the samples, a 3D view was chosen to better present the data. Table III indicates the results of the degradation modeling of the blends at four compositions by the Friedman technique, along with the experimental data. It was evident from the rs that the correlation was very good in a broad temperature range. All of the rs were higher than 0.99; this proved a good correlation of the analysis in the temperature range studied. The Freeman-Carroll method was also used to calculate the decomposition E_as and ns of all of the samples. The results of modeling by this method are listed in Table III. The values of the rs obtained by this method were more ill-fitting than those obtained from the other methods.

The E_a values from the models based on a single heating rate disclosed smaller amounts in comparison with models based on multiple heating rates. These models are applicable to single-rate-model quantities at lower E_as; it was significant that the degradation kinetics needed to apply different rate models. A kinetic study of the thermooxidation degradation of blends with different amounts of NBR and PC under stable air conditions and heating rates of 10, 20, and 30°C/min was done.

With the FWO method and different conversion values of α were compared with log β spot versus $1/T$. Figure 12 presents the E_a values. The curve for the P1 sample is depicted in Figure 12. It is noteworthy that the quantities resulting from the two different methods were close. The E_a and r results from both methods at 0.05 and 0.6° are reported in Table IV.

In this experiment, we used the KAS and FWO methods to obtain the E_as that were usable in all conversions in KAS with $\ln[(\beta/T^2]$, calculated by $1/T$, at different conversion ratios (α) and with line fitting on this spot. E_a was outcome. From the slope for these lines, the curves of the P1 sample are depicted in Figure 13.

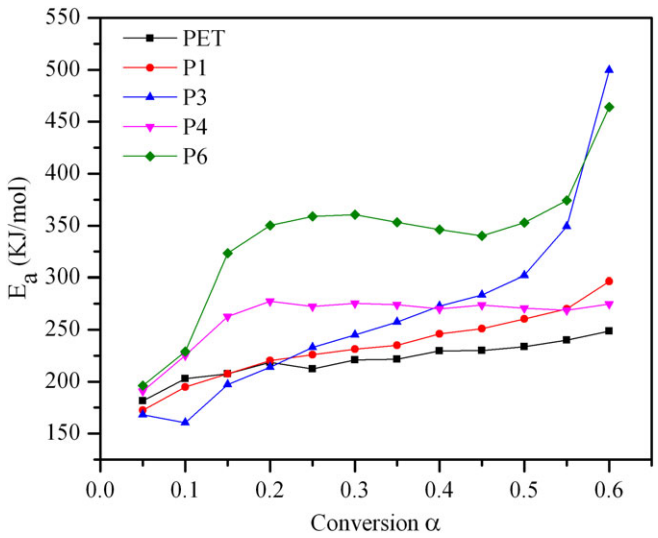

Figure 14. Plots of E_a versus the conversion for the samples of PET and the P1, P3, P4, and P6 blends calculated with the Friedman methods. [Color figure can be viewed at wileyonlinelibrary.com]

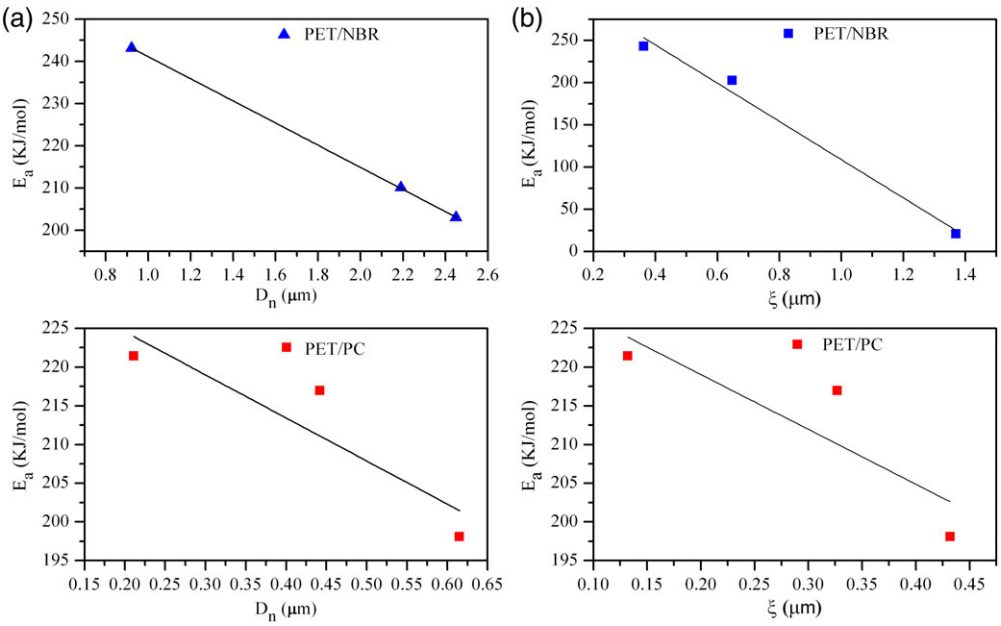

Figure 15. Plots of E_a versus the morphological parameters, (a) D_n and (b) ξ, for the PET–NBR and PET–PC blends. [Color figure can be viewed at wileyonlinelibrary.com]

According to the morphologies reported for the P1, P3, P4, and P6 samples in Figure 3 and 4, the values for E_a are given in Figure 14 for the PET, P1, P3, P4, and P6 samples. We concluded that sample P1, which displayed a miscible phase between PET and PC, as shown in the figure, revealed a smaller range compared to the P3 sample. With respect to the high difference in the weight percentage of PC phase in the P3 sample compared to P1 sample, the thermal stability in the P3 sample was enhanced. Additionally, a char-formation effect at high conversion ratios was obvious with the sudden increase in the E_a value. The effect of the PC addition amount on the reduction of the initiation of thermal degradation was apparent at lower conversion ratios ($\alpha \leq 0.2$). The E_a values versus the conversion ratios for sample P6 compared to sample P4, with a lower weight percentage of NBR phase (10 wt %), showed it to be a rubbery component with lower thermal stability and was reported in higher quantities. In fact, this function highly influenced the morphology of the samples. The higher E_a was due to the continuous morphology and the high phase reaction in sample P6 (Table IV).

Correlation of the Morphology with the Degradation E_a

The PC and NBR droplet sizes and inter-particle distances (ζs) were obtained on the basis of the following equations:

$$D_n = \sum N_i D_i / \sum D_i \tag{7}$$

$$\zeta = D_n\{[\pi/(6\varphi_d)]^{1/3} - 1\} \tag{8}$$

where D_n is the number-average droplet size (the calculated D_n values for the binary samples are shown in the SEM images in Figures 1 and 2), N_i is the frequency of a droplet with a diameter of D_i, and φ_d is the droplet phase volume fraction. D_n and ζ are among the morphological parameters influencing the blend thermal behavior. Therefore, the E_a values for the binary sample parameters are illustrated in Figure 15(A,B) to demonstrate these effects. Figure 15 (A) divulges the D_n effects of the PC and NBR dispersed phases on the thermal stability behavior. The resulting curves clearly indicated that with the reduction of D_n, E_a presented an increase in the thermal stability. According the particle distance effect shown in in Figure 15(B), the thermal stability was improved by the decrease in the particle distance. With the special morphology of ternary blend, quantitative study was impossible.

CONCLUSIONS

The SEM images of the binary samples divulged a matrix-dispersed morphology. Changing the composition ratios of the dispersed-phase particles showed differences in the ternary samples P1, P3, and P6 that were due to the occurrence of transesterification and exchange reactions during the mixing process and the formation of random copolymers; these demonstrated miscibility and reaction compatibility. The dynamic mechanical analysis results were strongly compatible with the SEM results of the ternary samples, which also showed miscibility. In the binary samples, a change in the loss peak place disclosed interactions between the phases. The TG and DTG data were analyzed kinetically by three different methods, each of which gave different apparent kinetic parameters. The TG results reported thermal degradation behavior of the pure, binary, and ternary samples. We observed how the miscibility between the PET and PC phases influenced the formation of random copolymers. Furthermore, the interactions between the hydroxyl and carboxyl end groups of PET with the nitrile groups of NBR led to the development of a single-stage degradation process in the samples. All of the test results show a high dependency of the morphological parameters on the thermal stability (T_{onset}, T_{50}, T_{max}, and E_a). The onset decomposition temperature is the temperature at which initial loss of mass was observed and Temperature at which 50 % mass loss was recorded by DTG. With respect to this report, the effects of the weight decrease on the dispersed-phase particles and

distance particles (binary samples) were obvious; a more stable and continuous (P6) morphology was formed with respect to increases in the thermal stability.

REFERENCES

1. Janowska, G.; Rybiński, P. *J. Therm. Anal. Calorim.* **2008**, *91*, 697.
2. Gupta, S.; Chowdhury, S. R.; Mishra, J. K.; Das, C. K.; Patra, P. K.; Tripathy, A. K.; Banerjee, M. S. *Mater. Lett.* **2000**, *46*, 125.
3. Giannelis, E. P. *Adv. Mater.* **1998**, *8*, 29.
4. Merinska, D.; Malac, Z.; Hrnicirik, J.; Simonik, J. *Soc. Plast. Eng. Annu. Tech. Conf. Pap.* **2001**, *47*, 2166.
5. Tuan, C. C.; Wu, F.; Moon, K. S.; Wong, C. P. Presented at the 2017 I.E. 67th Electronic Components and Technology Conference (ECTC), Orlando, FL, 30 May–2 June, **2017**.
6. Zhang, Y.; Park, S. J. *J. Polym. Sci. Part B: Polym. Phys.* **2017**, *55*, 1890.
7. Rozyanty, A. R.; Rozman, H. D.; Tay, G. S. *Adv. Mater. Res.* **2011**, *264*, 712.
8. George, S.; Varughese, K. T.; Thomas, S. *Polymer* **2000**, *41*, 5485.
9. Roeder, J.; Oliveira, R. V. B.; Becker, D.; Gonçalves, M. W.; Soldi, V.; Pires, A. T. N. *Polym. Degrad. Stab.* **2005**, *90*, 481.
10. Lizymol, P. P.; Thomas, S. *Polym. Degrad. Stab.* **1993**, *41*, 59.
11. Jose, S.; Selvin Thomas, P.; Thomas, S.; Karger-Kocsis, J. *Polymer* **2006**, *47*, 6328.
12. Stipanelov Vrandečić, N.; Klarić, I.; Kovačić, T. *Polym. Degrad. Stab.* **2004**, *84*, 31.
13. Friedman, H. L. *J. Polym. Sci. Polym. Symp.* **1964**, *6*, 183.
14. Flynn, J. H.; Wall, L. A. *J. Res. Nat. Bur. Stand.* **1966**, *70*, 487.
15. Ozawa, T. *J. Therm. Anal. Calorim.* **1970**, *2*, 301.
16. Doyle, C. *J. Appl. Polym. Sci.* **1962**, *6*, 639.
17. Kissinger, H. E. *Anal. Chem.* **1957**, *29*, 1702.
18. Popescu, C. *Thermochimica Acta.* **1996**, *285*, 309.
19. Dowdy, D. R. *J. Therm. Anal.* **1987**, *32*, 137.
20. Berki, P.; G#öbl, R.; Karger-Kocsis, J. *Polym. Test.* **2017**, *61*, 404.
21. Romhány, G.; Czigány, T.; Karger-Kocsis, J. *Polym. Rev.* **2017**, *57*, 397.
22. Colonna, S.; Bernal, M. M.; Gavoci, G.; Gomez, J.; Novara, C.; Saracco, G.; Fina, A. *Mater. Des.* **2017**, *119*, 124.
23. Paul, M. A.; Alexandre, M.; Degée, P.; #Henrist, C.; Rulmont, A.; Dubois, P. *Polymer* **2003**, *44*, 443.
24. Sahami, M.; Kalaee, M.; Aghili, A.; Mazinani, S.; Yeganeh, J. K. *J. Vinyl Addit. Technol.* **2017**, *23*, 180.
25. Al-Mulla, A.; Shaban, H. I. *Polym. Bull.* **2007**, *58*, 893.
26. Jang, B. N.; Wilkie, C. A. *Polym. Degrad. Stab.* **2004**, *86*, 419.
27. Swoboda, B.; Buonomo, S.; Leroy, E.; Cuesta, J. L. *Polym. Degrad. Stab.* **2007**, *92*, 2247.
28. Mendes, L. C.; Abrigo, R. E. R.; Ramos, V. D.; Pereira, P. S. C. *J. Therm. Anal. Calorim.* **2010**, *99*, 545.